Charles University in Prague, Faculty of Mathematics and Physics

Astronomical Institute (v. v. i.), Academy of Sciences of the Czech Republic, Observatory Ondřejov

Abstract of the doctoral thesis

Velocity fields in the solar photosphere

Michal Švanda

Supervisor: **RNDr. Michal Sobotka, CSc.**

Advisers: **Ing. Mirek Klvaňa, CSc.**, **RNDr. Pavel Ambrož, CSc.**

Prague, 2007

Universita Karlova v Praze, Matematicko-fyzikální fakulta

Astronomický ústav (v. v. i.), Akademie věd České republiky, observatoř Ondřejov

Autoreferát disertační práce

Rychlostní pole ve sluneční fotosféře

Michal Švanda

Školitel: **RNDr. Michal Sobotka, CSc.**

Konzultanti: **Ing. Mirek Klvaňa, CSc.**, **RNDr. Pavel Ambrož, CSc.**

Praha, 2007

Výsledky disertační práce byly získány během prezenčního doktorského studia na MFF UK v Praze v letech 2004 až 2007.

Uchazeč:

Mgr. Michal Švanda
Astronomický ústav (v. v. i.) AV ČR
Fričova 298
251 65 Ondřejov

Školitel:

RNDr. Michal Sobotka, CSc.
Astronomický ústav (v. v. i.) AV ČR
Fričova 298
251 65 Ondřejov

Školící pracoviště:

Astronomický ústav (v. v. i.) AV ČR
Fričova 298
251 65 Ondřejov

Oponenti:

Dr. Horst Balthasar
Astrophysikalisches Institut Potsdam
An der Sternwarte 16
D-14482 Potsdam
Germany

RNDr. Aleš Kučera, CSc.
Astronomický ústav
Slovenská akadémia vied
SK-059 60 Tatranská Lomnica
Slovak Republic

Autoreferát byl rozeslán dne 11. 11. 2007.

Obhajoba se koná dne 11. 12. 2007 v 9.00 před komisí obhajoby doktorských disertačních prací oboru *F1 – Teoretická fyzika, astronomie a astrofyzika* na MFF UK, Ke Karlovu 3, 121 16 Praha 2, v místnosti č. 105.

S disertací je možno se seznámit na studijním oddělení – doktorské studium MFF UK, Ke Karlovu 3, 121 16 Praha 2, nebo v elektronické verzi na adrese http://sirrah.troja.mff.cuni.cz/ svanda/disertace.pdf (PDF, 12 MB).

Předseda oborové rady F1:

Prof. RNDr. Jiří Bičák, DrSc.
Ústav teoretické fyziky MFF UK
V Holešovičkách 2
180 00 Praha 8

Obsah

Acknowledgements

Some parts of this thesis were made under an effective support of Czech Science Foundation under the grants No. 205/04/2129 and 205/03/H144, of Grant Agency of Academy of Sciences of the Czech Republic under grant No. IAA 3003404, and ESA-PECS under grant No. 98030. The data used in this thesis were kindly provided by the SoHO/MDI consortium (SoHO is the project of international cooperation between ESA and NASA) and NSO/Kitt Peak, which are produced cooperatively by NSF/NOAO, NASA/GSFC, and NOAA/SEL.

1 Introduction

The Sun is the closest star – this fact allows us to resolve individual features on its surface and in its atmosphere. Using many types of observations, we can collect a large amount of data describing the behaviour of the solar plasma in various phenomena. The Sun is a variable star – the magnetic activity undergoes the main cycle with a length of 22 years (reversal of a global magnetic field) which is composed of two consecutive 11 years 'spot' cycles. The most visible evidence of the solar cyclicity is the change of the number, size, and shape of sunspots. However, evidences of such cyclicity may be found also in the total solar irradiance, number of solar flares, or the shape of the solar corona. The Sun exhibits also cycles with other lengths (from few minutes to many centuries) and different properties. Better knowledge of the physics lying under solar magnetic variability and active phenomena will improve our attempts to predict solar activity.

The first evidence about the velocity fields in the solar photosphere comes from Christoph Scheiner, who in 1630 noticed that sunspots near the equator traverse the solar disc faster than sunspots in higher latitudes. Carrington (1859) used series of sunspot drawings to infer the differential rotation rate and the inclination of the solar rotation axis. Since Carrington's measurement of the differential rotation this phenomenon was confirmed many times using many techniques. For details see an older review by Schröter (1985) or a recent review by Beck (2000). The existence of the differential rotation was the first evidence about the movements of objects in the solar photosphere. Since then many other types of motions of a complex and vigorous nature were detected.

Except for the granulation (convection cells with characteristic size of 1 Mm and lifetime of 3–17 minutes), the supergranulation is visible i. e. in full-disc dopplergrams (typical size of 30 Mm, lifetime of ∼24 hours). The largest-scale velocity fields consist of the differential rotation and meridional circulation. The differential rotation is defined as an integral of the zonal (east–west) component of the velocity field depending on the solar latitude, b, and radius. The meridional flow on the contrary is calculated as an integral of the north–south component of the velocity field, generally depending again on the latitude and radius. Both, the differential rotation and meridional circulation, are the key ingredients of the solar dynamo. The differential rotation plays an important role in generating and strengthening of toroidal magnetic field inside the Sun, while the meridional flow transports the magnetic flux towards the solar poles resulting in cyclic polar field reversals.

The most substantial recent advance in the search for large-scale non-axisymmetric motions in the solar envelope has been the mapping of horizontal flows by local helioseismology. After subtracting out the contributions from the differential rotation and meridional circulation, the residual flow maps reveal intricate, evolving flows on a range of spatial scales (e. g. Zhao & Kosovichev, 2004). Such flow patterns have become known as solar subsurface weather, SSW (Toomre, 2002). Such maps derived using different local helioseismic inversions (ring diagram or time-distance) are within the resolution quite stable (Hindman et al., 2004).

1.1 Methods of measurements of the large-scale velocity fields

Basically, there are three methods for measuring of the photospheric velocity fields:

1. *Direct Doppler measurement* – provides only one component (line-of-sight) of the velocity vector. These velocities are generated by local photospheric structures, amplitudes of which are significantly greater than amplitudes of the large-scale velocities. The complex topology of such structures complicates an utilisation for our purpose. Analysing this component in different parts of the solar disc led to very important discoveries (e. g. supergranulation – Hart, 1956 and Leighton et al., 1962).

2. *Tracer-type measurement* – provides two components of the velocity vector. When tracing some photospheric tracers, we can compute the local horizontal velocity vectors in the solar photosphere. Tracking motions of sunspots across the solar disc led to the discovery of the differential rotation (Carrington, 1859).

3. *Local helioseismology* – provides a full velocity vector. The local helioseismology (see Kosovichev, 1996, Zhao et al., 2001, or Zhao & Kosovichev, 2004) is a very promising method using the information about the solar oscillations to infer the structure and also the dynamics in the convection zone.

In this work we used mostly the tracer type method, local correlation tracking in particular, applied to the surface structures.

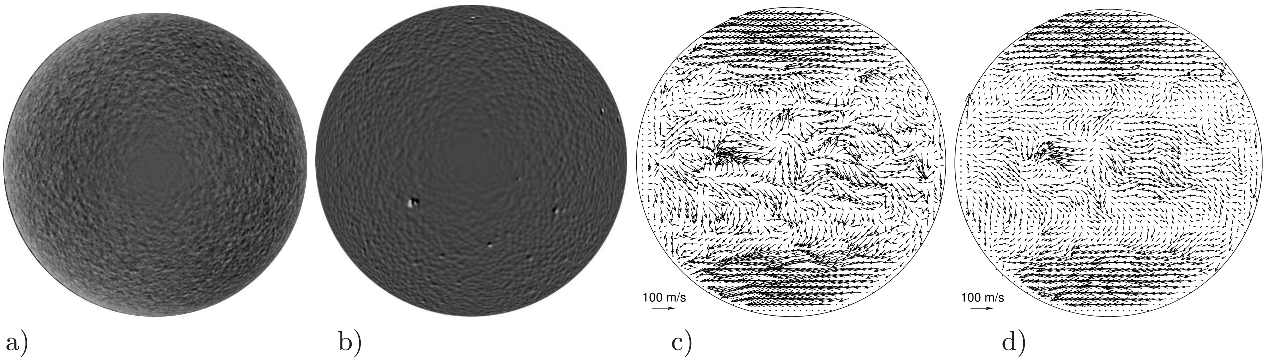

Figure 1: *a)* – the measured MDI dopplergram, *b)* – the dopplergram produced by SISIOD code, *c)* – the model velocity field introduced in the synthetic data, *d)* – the resulting velocity field after the whole procedure look very similar to the model one.

The method needs a tracer – a significant structure recorded in different frames, the lifetime of which is much longer than the time lag between the correlated frames. We decided to use the supergranulation pattern in the full-disc dopplergrams, acquired by the Michelson Doppler Imager (MDI; Scherrer et al., 1995) onboard Solar and Heliospheric Observatory (SoHO). We assume that supergranules are carried as objects by the large-scale velocity field. This velocity field is probably located beneath the photosphere, so that the resulting velocities will describe the dynamics in both the photospheric and subphotospheric layers. The existence of the supergranulation on almost the whole solar disc (in contrast to magnetic structures) and its large temporal stability make the supergranulation an excellent tracer.

1.1.1 Local correlation tracking

Since the photosphere is a very thin layer (0.04 % of the solar radius), the large-scale photospheric velocity fields have to be almost horizontal. Then, the tracer-type measurement should be sufficient for mapping the behaviour of such velocities. In this field the local correlation tracking (LCT) method is very useful.

This method was originally designed for the removal of the seeing-induced distortions in image sequences (November, 1986) and later used for mapping the motions of granules in the series of white-light images (November & Simon, 1988) under the name *local cross-correlation*. The method works on the principle of the best match of two frames that record the tracked structures at two different instants.

The algorithm is applicable to two frames I_1 and I_2 having the same dimension that were captured in different instants. There is a time lag τ between both frames, which has to be smaller that the lifetime of used tracer. For every pixel in the first frame a subframe (correlation window) is chosen, described by the coordinates of its centre (x_0, y_0) and the size p. Since in this study we used the Gaussian-weighted window, p is equal to the $FWHM$ of the Gaussian profile. The parameter p is selected according to used tracer, so that p is larger than a characteristic size of the tracer. Let the subframe in image I_1 is $S_1(x_0, y_0)$.

$S_1(x_0, y_0)$ is compared with a subframe in image I_2 of the same size, which has its centre in the coordinates $(x_0 + \delta x, y_0 + \delta y)$. Let the subframe in image I_2 is $S_2(x_0 + \delta x, y_0 + \delta y)$. The proper motion of tracers in the point (x_0, y_0) is defined by a displacement $(\delta x, \delta y)$, which maximise the correlation of S_1 and S_2. LCT was recently used for tracking many features in various types of observations, especially for tracking the granules in high-resolution white-light images (e.g. Sobotka et al., 1999). The same method was recently used for calculation of large-scale flow fields using low-resolution magnetograms (e.g. Ambrož, 2001).

2 Method and tests on synthetic data

A recent experience with applying the LCT method to observed data (e.g. Švanda et al., 2005) has shown that for the proper setting of the parameters and for the tuning of the method, synthetic (model) data with known properties are needed. The synthetic data for the analysis come from a simple numerical simulation (SISOID code = *SI*mulated *S*upergranulation as *O*bserved *I*n *D*opplergrams) with the help of which we can reproduce the supergranulation pattern in full-disc dopplergrams. The SISOID code is not based on physical principles taking place in the origin and evolution of supergranulation, but instead on a reproduction of known properties that describe the supergranulation (see Fig. 1*a* and *b*). The design of the synthetic dopplergrams with known parametres is very important for the calculation of the vector

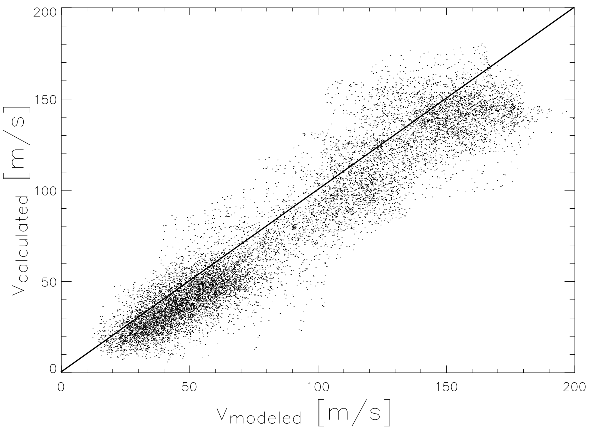

Figure 2: Scatter plot for inference of the calibration curve. Magnitudes of calculated velocities are slightly underestimated by LCT, but the linear behaviour is clearly visible. A line representing the 1:1 ratio is displayed. The calibration affects only the magnitudes of the flows, while the directions do not need any correction.

velocity fields, so that we carried out the simulation carrefully to get the correct and valuable results about the abilities of the method.

The model velocity field with Carrington rotation added is applied according to the assumption of the velocity analysis that the supergranules are carried by a velocity field on a larger scale. In the simulation, the position of individual supergranules is influenced, and no other phenomena are taken into account. These synthetic dopplergrams are visually similar to the real observed dopplergrams.

In our tests we have used lots of variations of simple axisymmetric model flows (with a wide range of values of parameters describing the differential rotation and meridional circulation) with good success in reproducing the models. When comparing the resulting vectors of motions with the model ones, we found a systematic offset in the zonal component equal to $v_{\mathrm{offset,\ zonal}} = -15\ \mathrm{m\,s^{-1}}$. This constant offset appeared in all the tested model velocity fields and comes from the numerical errors during the "derotation" of the whole time series. For the final testing, we used one of the velocity fields obtained in our previous work (Švanda et al., 2005). This field approximates the velocity distribution that we may expect to observe on the Sun (see Fig. 1*c*). The model flows have structures with a typical size of 60″, since they were obtained with the correlation window of this size.

The calculated velocities (with $v_{\mathrm{offset,\ zonal}} = -15\ \mathrm{m\,s^{-1}}$ corrected) were compared with the model velocities (Fig. 1*c* and *d*). Already from the visual impression it becomes clear that most of vectors are reproduced very well in the direction, but the magnitudes of the vectors are not reproduced so well. Moreover, it seems that the magnitudes of vectors are underestimated. This observation is confirmed when plotting the magnitudes of the model vectors versus the magnitudes of the calculated vectors (Fig. 2). The scatter plot contains more than 1 million points, and most of the points concentrate along a strong linear dependence, which is clearly visible. This dependence can be fitted by a straight line that can be used to derive the calibration curve of the magnitude of calculated velocity vectors. The calibration curve is given by the formula

$$v_{\mathrm{cor}} = 1.13\, v_{\mathrm{calc}}, \tag{1}$$

where v_{calc} is the magnitude of velocities coming from the LCT, and v_{cor} the corrected magnitude. The directions of the vectors before and after the correction are the same. The uncertainty of the fit can be described by 1-σ-error 15 $\mathrm{m\,s^{-1}}$ for the velocity magnitudes under 100 $\mathrm{m\,s^{-1}}$ and 25 $\mathrm{m\,s^{-1}}$ for velocity magnitudes greater than 100 $\mathrm{m\,s^{-1}}$. The uncertainties of approx. 15 $\mathrm{m\,s^{-1}}$ have their main origin in the evolution of supergranules. Using the synthetic data generated by the SISOID code we have verified that the proposed method is reliable when measuring the large-scale velocity fields in the solar photosphere using the LCT method applied to full-disc dopplergrams.

For the study we have processed all suitable data measured by MDI. The instrument observed full-disc dopplergrams approximately two months each year in a high cadence of one frame per minute. These *Dynamic campaigns* provide suitable material for our method. Between May 23, 1996 and May 22, 2006 we have 806 days covered by high-cadence measurements. In each of these days, two 24-hour averages sampled every 12 hours were calculated. In some days, MDI had significant gaps in measurements, so in such cases we did not have enough homogeneous material to process. Therefore, in all the *Dynamic campaigns* 502 days were useful for our analysis and we calculated 1004 full-disc horizontal velocity fields. The processing of almost 3 TB of primary data took several months using fast computers running in the network of W. W. Hansen Laboratory, Stanford University.

The data were processed following an ongoing procedure. The method processes 24-hours series of MDI full-disc dopplergrams, containing 1 440 frames. The one-day series first undergoes the noise and disturbing effects removal. From all frames, the line-of-sight component of the Carrington rotation is subtracted and the effect of a perspective is corrected. The frames are transformed so that the heliographic latitude of the disc centre $b_0 = 0$ and the position angle of the solar rotation axis $P = 0$. Then, the p-modes of the solar oscillations are removed using a weighted average (see Hathaway, 1988). The weights have a Gaussian form given by the formula:

$$w(\Delta t) = e^{\frac{(\Delta t)^2}{2a^2}} - e^{\frac{b^2}{2a^2}} \left(1 + \frac{b^2 - (\Delta t)^2}{2a^2}\right), \tag{2}$$

where Δt is a time distance of a given frame from the central one (in minutes), $b = 16$ minutes and $a = 8$ minutes. We sample averaged images in the interval of 15 minutes. The filter suppresses more than five hundred times the solar oscillations in the 2–4 mHz frequency band.

The processing of averaged frames consists of two main steps. In the first main step the mean zonal velocities are calculated and, on the basis of expansion to the Fay's formula $\omega = c_0 + c_1 \sin^2 b + c_2 \sin^4 b$, the differential rotation is removed. In the second main step, the LCT algorithm with an enhanced sensitivity is applied. Finally, the differential rotation (obtained in the first step) is added to the vector velocity field obtained in the second main step. Both main steps can be divided into several sub-steps, which are mostly common.

1. The data series containing 96 averaged frames is "derotated" using the Carrington rotation rate in the first step and using the calculated differential rotation in the second step.

2. Derotated data are transformed into the Sanson-Flamsteed coordinate system to remove the geometrical distortion caused by the projection to the disc. The Sanson-Flamsteed (also known as sinusoidal) pseudo-cylindrical projection conserves the areas and therefore is suitable for the preparation of the data used by LCT.

3. Remapped data undergoes the k-ω filtering (e. g. Title et al., 1989) with the cut-off velocity $1\,500\ \mathrm{m\,s^{-1}}$ for suppression of the noise coming from the evolutionary changes of supergranules, of the numerical noise, and for the partial removal of the "blind spot" (an effect at the centre of the disc, where the supergranular structures are almost invisible in dopplergrams due to the prevailing horizontality of their internal velocity field).

4. Finally, the LCT is applied: the lag between correlated frames is 4 hours, the correlation window has $FWHM$ $60''$, the measure of correlation is the sum of absolute differences and the nine-point method for calculation of the subpixel value of displacement is used. The calculated velocity field is averaged over the period of one day.

5. The resulting velocity field is corrected using the formula (1). The directions of the vectors before and after the correction are the same. Finally, v_x component is corrected for the data-processing bias of $-15\ \mathrm{m\,s^{-1}}$.

3 Direct comparison to the time-distance helioseismology

The most modern method of the measurements of surface and sub-surface velocity fields is a local helioseismology. We decided to compare the results obtained by this method and our method using the same dataset. The results of both methods can be interpreted differently. While local helioseismology measures intrinsic plasma motions (through advection of acoustic waves), LCT measures apparent motions of structures. It is known that some structures do not necessarily follow the flows of the plasma on the surface. For example, supergranulation appears to rotate faster than the plasma (Beck & Schou, 2000), which may be caused by travelling waves (Gizon et al., 2003) or may be explained also as projection effect (Hathaway et al., 2006). Some older studies (see e. g. Rhodes et al., 1991) also suggest that the difference in flow properties measured on the basis of structures motions and plasma motions is caused by deeper anchor depth of these structures. An evolution of pattern may also play significant role (e. g. due to emergence of magnetic elements). Another possibility is that surface structures are not coherent features, but patterns traveling with a different group velocity than the surface plasma velocity, such as occurs for the features present in simulations of travelling-wave convection (e. g. Hurlburt et al., 1996).

The selected dataset consists of 27 data-cubes from March 12th, 2001, 0:00 UT to April 6th, 2001, 0:31 UT, where each third day was used, and in these days three 8.5-hour long data-cubes were processed (so that every third day in the described interval was fully covered by measurements). Each data-cube is

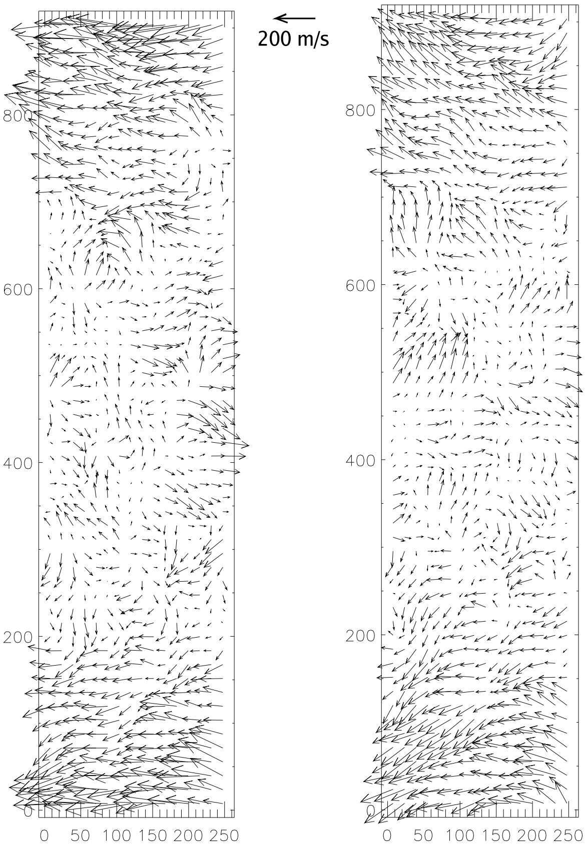

Figure 3: *Left* – velocity field obtained by the LCT method. *Right* – vector field obtained by the time-distance technique. Both plots are centered at heliographic coordinates $b_0 = 0.0^\circ$, $l_0 = 214.3^\circ$, units on both axes are pixels in the data frame with resolution $0.12^\circ\,\mathrm{px}^{-1}$ in the Postel projection.

composed of 512 dopplergrams (with spatial resolution of $1.98''\,\mathrm{px}^{-1}$) at a one-minute cadence (so that covering 8 hours and 32 minutes). All the frames of each data-cube were tracked with a rigid rate of $2.871\ \mu\mathrm{rad\,s}^{-1}$, remapped to the Postel projection with a resolution of $0.12^\circ\,\mathrm{px}^{-1}$ (1,500 $\mathrm{km\,px}^{-1}$ at the centre of the disc), and only a central meridian region was selected for the ongoing processing (with size of 256×924 px covering 30 heliographic degrees in longitude and running from -54° to $+54^\circ$ in latitude), so that effects of distortions due to the projection do not play a significant role.

The results of the comparison were statistically processed to obtain the cross-calibration curves for these methods. We have confirmed the underestimation of the calculated velocity field by LCT with the factor, which is in perfect agreement with Eq. (1). Moreover, we have found an asymmetry in the time-distance results, when the meridional component is about 2-times underestimated in comparison to a zonal component. We found two possibilities that could explain this behaviour. The first explanation is a drift of the supergranular pattern towards the equator. This case does not explain why the meridional velocities from both techniques seem to be proportional to each other. A systematic drift would rather be depicted as a systematic constant shift, or a shift depending on the latitude. However, the meridional component of velocities is generally rather small, so that the errors of the measurements can play a significant role and the proportional behavior can be only apparent.

The second explanation is based on unspecified asymmetries influencing travel-time measurements, for instance, due to different sensitivity of the MDI instrument to p-modes propagating in the east-west and north-south directions. As it has been studied recently (Georgobiani et al., 2007), a comparison between f-mode time-distance and LCT applied to realistic numerical simulation did not show such asymmetry. The asymmetry in the east-west and north-south directions observed by time-distance helioseismology was on the contrary noticed in a recent study based on numerical simulated data (Zhao et al., 2007). So that the asymmetry takes place only in the p-modes inversions and should be investigated in more details further.

For a detailed comparison of the flow fields, we selected one data cube, representing 8.5-hour measurements centered at 4:16UT of March 24th, 2001 (l_0=214.3°). In this map, the correlation coefficient for the x-component of the velocity is $\rho = 0.82$ and for the y-component $\rho = 0.58$, and for the vector magnitude $\rho = 0.73$. The vector plots of the flow fields obtained by both techniques, shown in Fig. 3, seem to be quite similar in general; however many differences can be seen. The regions where the differences are most significant correspond to relatively small (under 50 $\mathrm{m\,s}^{-1}$) velocities.

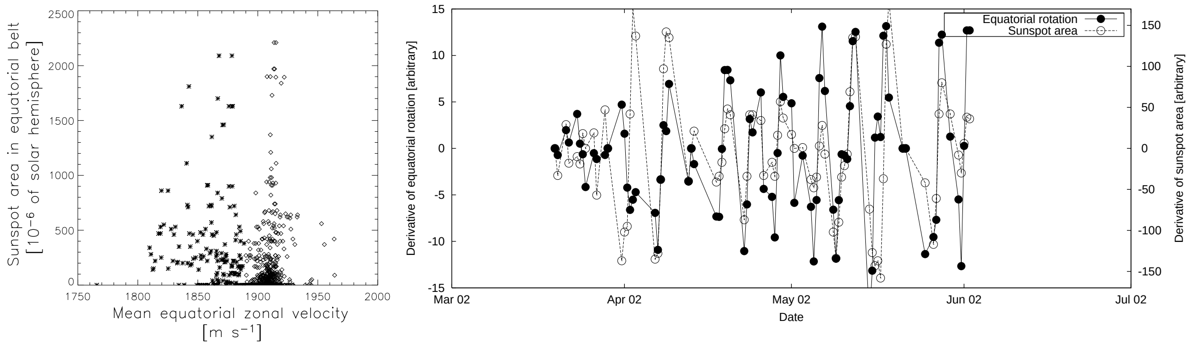

Figure 4: *Left* – Mean zonal equatorial velocity versus the sunspot area in the near-equatorial belt. We decided to divide the data in two regimes along the velocity axis. Although the division is arbitrary, we believe that it is supported by the theory of the dynamical disconnection of sunspots from their roots. *Right* – Derivatives of the mean zonal velocity (solid curve) and the sunspot area in the near-equatorial region (dashed curve) in 2002. Both quantities correlate with each other quite nicely.

4 Long-term behaviour

We have verified that the method developed and tested using the synthetic data is suitable for application to real data obtained by the MDI onboard SoHO and maybe also to the data that will be produced by its successor Helioseismic Michelson Imager (HMI) onboard the Solar Dynamic Observatory (SDO). HMI will have a greater resolution and will cover larger time span than two months each year. We verified that the long-term evolution of the horizontal velocity fields measured using our method is in agreement with generally accepted properties, displaying the diferential rotation, poleward mean meridional flow, and torsional oscillations pattern.

The mean zonal and meridional components in the equatorial area (averaged in the belt $b = -5\,^\circ - +5\,^\circ$) were analysed in order to examine the periods contained in the data. Since the data are not equidistant at all, a simple harmonic analysis cannot be used, so that the *Stellingwerf method* (Stellingwerf, 1978) was applied. Unfortunately, it has to be concluded that no significant period in the available data set was detected, except for two suspicious ones. Their values are 657 days (1.80 years) in the meridional component and 1712 days (4.69 years) in the zonal component. Note that the 1.8-year period was also detected by Knaack et al. (2004). It is claimed to be related to a possible Rossby wave r-mode signature in the photosphere with azimuthal order $m \sim 50$ reported by Kuhn et al. (2000). The period estimate for such an r-mode is close to 1.8 years. According to Knaack et al. (2005), such a periodicity was observed in the total magnetic flux only on the southern hemisphere from 1997 to 2003. The coupling between the zonal flow and the meridional circulation could transfer the signal of the r-mode motion to the mean meridional component.

The coupling of equatorial zonal velocity (average equatorial solar rotation) and the solar activity in the near-equatorial area (belt of heliographic latitudes from $-10\,^\circ$ to $+10\,^\circ$) was also investigated. The average equatorial zonal velocity incorporates the average supergranular network rotation and also the movement of degenerated supergranules influenced by a local magnetic field with respect to their non-magnetic vicinity. Indexes of the solar activity were extracted from the daily reports made by *Space Environment Center National Oceanic and Atmospheric Administration (SEC NOAA)*. Only the days when the measurements of horizontal flows exist were taken into account. As the index of the activity we have considered the total area of sunspots in the near-equatorial belt and also their type.

First of all, the correlation coefficient ρ between the mean equatorial zonal velocity and the sunspot area in the near-equatorial belt was computed with a value of $\rho = -0.17$. There is no significant linear relation between these two indices. The dependence of both quantities is plotted in Fig. 4 left. There can be clearly found two different regimes, which are divided by the velocity of approximately 1890 $\mathrm{m\,s^{-1}}$. In one regime (77 % of the cases), the equatorial belt rotates about 60 $\mathrm{m\,s^{-1}}$ faster (1910 ± 9 $\mathrm{m\,s^{-1}}$; hereafter a “fast group”) than the Carrington rotation, in the other one (23 %) the rotation rate is scattered around the Carrington rate (1860 ± 20 $\mathrm{m\,s^{-1}}$; hereafter a “scattered group”). The division in these two suggested groups using the speed criterion is arbitrary. Detailed studies of the sunspot drawings obtained from the Patrol Service of Ondřejov Observatory and the Mt. Wilson Observatory drawings archive revealed that in the “fast” group, the new or growing young active regions were present in the equatorial belt. On the contrary, in the “scattered” group the decaying or recurrent active regions prevailed in the equatorial area.

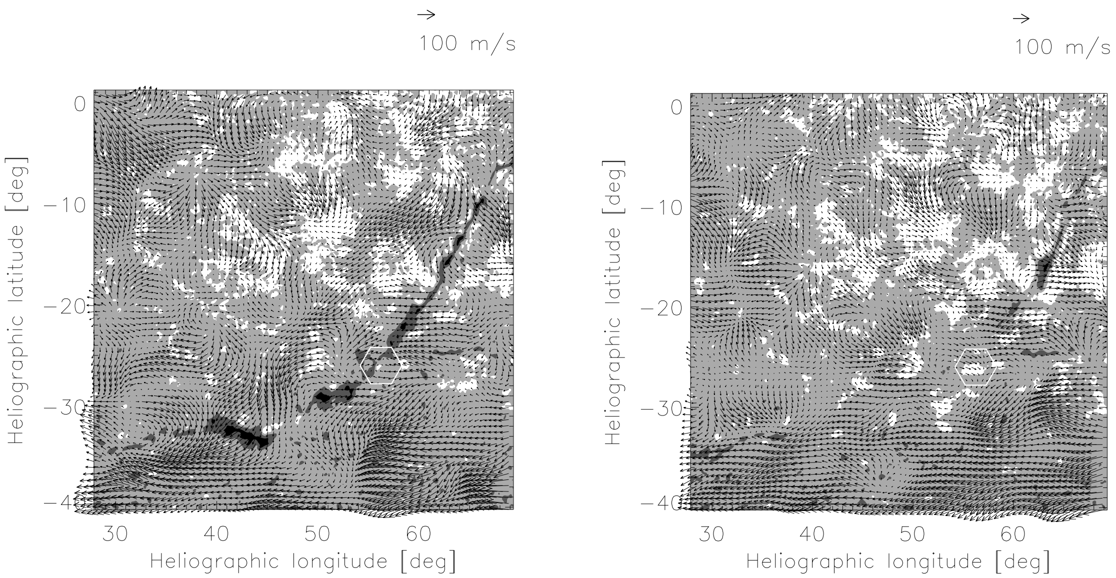

Figure 5: Horizontal motions in the area of the eruptive filament measured before (*left*) and after (*right*) the eruption. The filament observed by ISOON on October 7 2004 at 13:30 UT is superimposed. The site of the starting point is marked by hexagon.

The observed behaviour could be a manifestation of the disconnection of magnetic field lines from the base of the surface shear during the evolution of the growing sunspot group. This behaviour was theoretically studied by Schüssler & Rempel (2005). They suggested the dynamical disconnection of bipolar sunspot groups from their magnetic roots deep in the convection zone by upflow motions within three days after the emergence of the new sunspot group.

We have also studied how the presence of the magnetic active areas will influence the average flow field. Since we found that a direct correlation is weak due to the existence of two different regimes, we decided to study the temporal change of both quantities. The aim is to study whether an emerging active region in the near-equatorial belt will influence the average equatorial rotation. We computed numerical derivatives of the total sunspot area in the near-equatorial belt and of the average zonal equatorial flow. We have found that the correlation coefficient between both data series is $\rho = 0.36$ and is higher for the "fast group" ($\rho = 0.41$) than for the "scattered group" ($\rho = 0.24$). The correlation is higher in periods of increased magnetic activity in the equatorial belt. For example, for data in the year 2001 the correlation coefficient is $\rho_{2001} = 0.58$ and for the year 2002 $\rho_{2002} = 0.52$; see Fig. 4 right. In both particular cases, the correlation is higher for the "fast regime" ($\rho \sim 0.7$) than for the second group. In most cases, "spotty" equatorial belts seem to rotate slower than the average for the whole data series. However, it is clear that emerging active regions cause in most cases the increase of the rotation rate. This is in agreement with a generally accepted statement found first by Howard & Harvey (1970). The relation, obtained using a linear fit on our data set, can be described by the equation

$$\Delta v \sim 0.2\,\Delta A_{\mathrm{sunspots}}\ \mathrm{m\,s^{-1}}, \tag{3}$$

where Δv is a change of the equatorial rotation speed with respect to the Carrington rotation and $\Delta A_{\mathrm{sunspots}}$ is a change of sunspot area in the equatorial belt (in 10^{-6} of solar hemisphere). We estimate that strong local magnetic areas rotate few tens of $\mathrm{m\,s^{-1}}$ faster than the non-magnetic surroundings.

5 Motions around the footpoints of the eruptive filament

Dynamic processes on the Sun are linked to the evolution of the magnetic field as it is passing through the different layers from the convection zone to the solar atmosphere. In the photosphere, magnetic fields are subject to diffusion due to supergranular flows and to the large-scale motions of differential rotation and meridional circulation. The action of these surface motions on magnetic fields plays an important role in the formation of large-scale filaments (Mackay & Gaizauskas, 2003). In particular, the magnetic fields that are transported across the solar surface can be sheared by dynamic surface motions,

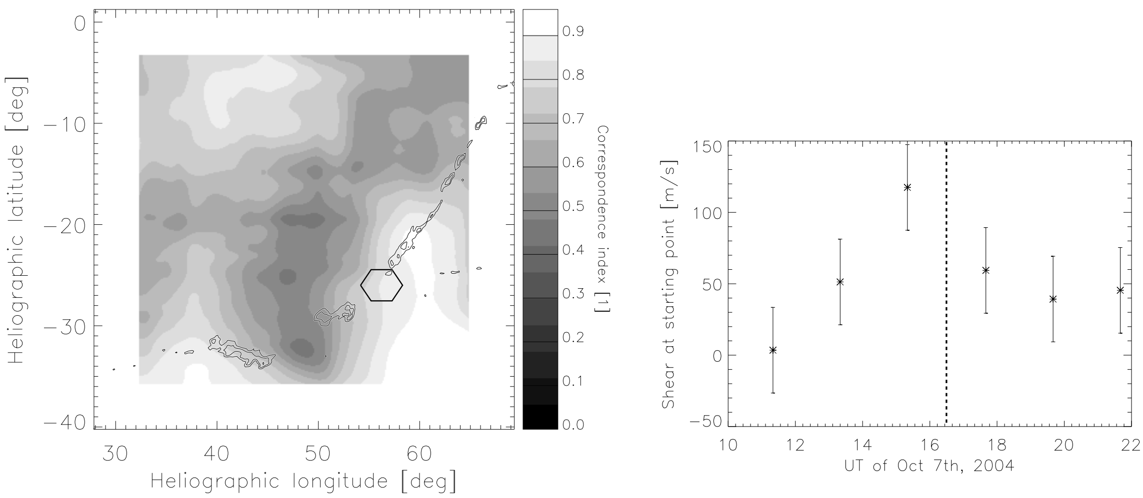

Figure 6: *Left* – The differences in the directions of both vector fields are evaluated using the weighted cosine of argument differences in the sliding window with size of 3.5 heliographics degrees. It is seen that the worst correspondence of both vector fields is in the area of the north–south current. It demonstrates that the flow field in the field of view remained more-or-less stable during the filament eruption except for the close vicinity of the starting point. *Right* – Temporal evolution of the velocity shear in zonal components. The eruption of filament took place at 16:30 UT.

which result in shearing of the coronal field. This corresponds to the formation of coronal flux ropes in models which can be compared with Hα filament observations (Mackay & van Ballegooijen, 2006). Many theoretical models try to reproduce the basic structure and the stability of filaments by taking into account surface motions as quoted above. These models predict that magnetic flux ropes involved in the solar filament formation may be stable for many days and then suddenly become unstable resulting in a filament eruption. Observations show that twisting motions are a very common characteristic of eruptive prominences (see for example Patsourakos & Vial, 2002).

During three consecutive days of the JOP 178 campaign, Oct 6, 7, and 8, 2004 (http://gaia. bagn.obs-mip.fr/jop178/index.html), we observed the evolution of a filament that was close to the central meridian. We also observed the photospheric flows directly below the filament and in its immediate area. The filament extended from $-5°$ to $-30°$ in latitude. A filament eruption was observed on October 7, 2004 at 16:30 UT in multiple wavelengths from ground and space instruments. The eruption produced a Coronal Mass Ejection (CME) at approximately 19:00 UT that was observed with LASCO-2/SOHO and two ribbon flares observed with SOHO/EIT. MDI/SOHO longitudinal magnetic field and Doppler velocity were recorded with a cadence of one minute during the 3 days. The Air Force ISOON telescope located at the National Solar Observatory/Sacramento Peak provided a full-disc Hα image every minute. The pixel sizes were respectively $1.96''$ for MDI magnetograms and dopplergrams and $1.077''$ for ISOON Hα images. Our primary goal was to derive the horizontal flow field below and around the filament.

The local correlation tracking technique was applied to the set of full-disc MDI dopplergrams measured in three days around the time of filament eruption in high cadence. Due to the time series length and the required temporal resolution we had to adjust some parameters of data processing. The most significant difference is a sampling of averaged p-modes-free frames in 1-minute cadence instead of 15 minutes.

Fig. 5 displays the horizontal flows before and after the eruption in a wide field of view measured using the LCT method on supergranular structures and averaging the resulting velocities over 3 hours. Before the eruption, we can clearly see the north–south stream parallel to and about $10°$ to the east of the filament. This stream disturbs differential rotation and brings plasma and magnetic structures to the south. Although differential rotation tends to spread the magnetic lines to the east, the observed north–south stream tends to shear the magnetic lines. After the eruption, only a northern segment of the filament is visible and the north–south stream has disappeared (cf. Fig. 5 and 6).

The observed north–south stream has an amplitude of 30–40 $\mathrm{m\,s^{-1}}$. In the sequence of Hα images that record the filament's evolution, the part of the filament, which is in the north–south stream, is rotated in a direction compatible with the flow direction of the stream. This behavior suggests that the foot-points of the filament are carried by the surface flows. The influence of the stream is strengthened by differential rotation. We should keep in mind that the filament extends from $-5°$ to $-30°$ in latitude and that the northern part of the filament is subjected to a faster rotation than the southern part. The stream, with a contribution of the differential rotation, causes the stretching of the coronal magnetic field in the filament and therefore contributes to destabilisation of the filament.

The shear in the zonal component at the point where the eruption started ($l = 56°$, $b = -26°$ in Carrington coordinates) is clearly visible and prevails before and after the eruption. We measured the shear as a difference between the mean zonal component v_x in with a side of 2.3° located 2.9° to the north and to the south of the point where the filament eruption appeared to start. The evolution in the shear velocity measured as the difference between the mean flow in the two boxes as a function of time can be seen in Fig. 6 right. Six 2-hours averages of the flow fields were used to determine this figure. One can see that the shear velocity is increasing before the eruption and decreasing after the eruption. One hour before the eruption, the shear reached the value of (120 ± 15) $\mathrm{m\,s^{-1}}$ in a distance of 5.2° (62 000 km in the photosphere). After the filament eruption, we observe a restoration of an ordinary differential rotation below $-30°$ in latitude.

The features observed in the topology of the horizontal velocity fields at the starting-point site could contribute to destabilisation the filament resulting in its eruption. We propose that the stability and evolution of filaments are influenced by surface flows that carry the footpoints of the filament.

6 Meridional magnetic flux transport

The largest-scale velocity fields on the Sun consist of the differential rotation and meridional circulation. Both, the differential rotation and meridional circulation, are the key ingredients of the solar dynamo. The differential rotation plays an important role in generating and strengthening of toroidal magnetic field inside the Sun, while the meridional flow transports the magnetic flux towards the solar poles resulting in cyclic polar field reversals (for a recent review, see Brandenburg & Subramanian, 2005).

The meridional flux transport seems to be an essential agent influencing the length, strength, and other properties of the solar magnetic cycles. Generally, the slower the meridional flow, the longer the next magnetic cycle can be expected. Dynamo models showed that the turn-round time of the meridional cell is between 17 and 21 years, and that the global dynamo may have some kind of memory lasting longer than one cycle (Dikpati et al., 2006).

The speed of the meridional flow and its variation with the solar cycle measured by local helioseismology in the subsurface layers of the Sun are used as an input in the recent flux-transport models. In local helioseismology measurements (e.g. Zhao & Kosovichev 2004, González Hernández et al. 2006), the meridional flow is derived from a general subsurface flow field by averaging the north-south component of plasma velocity over longitude for a Carrington rotation period. The studies reveal that the mean meridional flow varies with the solar activity cycle. These variations may significantly affect solar-cycle predictions based on the solar dynamo models, which assume that the magnetic flux is transported with the mean meridional flow speed (Dikpati & Gilman, 2006).

Our goal is to verify this assumption and to investigate the relationship between the subsurface meridional flows and the flux transport. In this study, we show that the mean meridional flows derived from the time-distance helioseismology subsurface flow maps are affected by strong local flows around active regions in the activity belt. However, these local flows have much less significant effect on the magnetic flux transport.

The magnetic field data were obtained from Kitt Peak synoptic maps of longitudinal magnetic field. The magnetic butterfly diagram is continuously constructed from synoptic magnetic maps measured at National Solar Observatory by averaging the magnetic flux in longitude at each latitude position for each solar rotation since 1976. At mid-latitudes of the magnetic butterfly diagram (Fig. 7 upper panel), between the active region zone and polar regions, we clearly see elongated structures corresponding to the poleward magnetic flux transport. The aim of our method is to measure the slopes of these structures and to derive the speed of the meridional magnetic flux transport.

In addition to the large-scale structures, the original diagram contains small-scale relatively short-living local magnetic field structures, which appear as a 'noise' in the diagram. To improve the signal-to-noise ratio for the magnetic flux structures we applied a frequency band-pass filter for the frequencies between 1.06×10^{-8} $\mathrm{s^{-1}}$ (period of 1093 days) and 3.17×10^{-7} $\mathrm{s^{-1}}$ (period of 36.5 days). The filtering procedure is performed separately for each individual latitudinal cut on the diagram. We tried also other methods of enhancement of structures and found that they all provide comparable results. The difference between the original butterfly diagram and the filtered one can be seen in Fig. 7 (upper and middle panel).

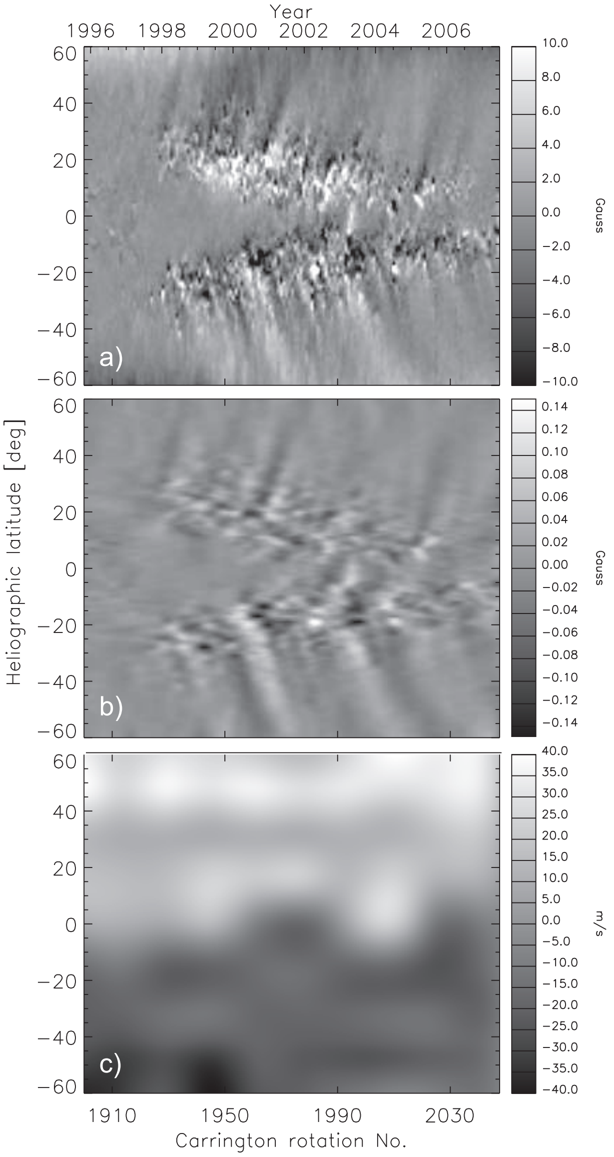

Figure 7: *a)* The magnetic butterfly diagram for cycle 23. *b)* The filtered magnetic butterfly diagram showing enhancements of the flux transport elongated structures. *c)* The measured meridional flux transportation speed (in the south–north direction) for Carrington rotations 1900–2048.

The meridional flux transport is measured on the basis of cross-correlation of two latitudinal rows in the map. We assume that the flux-transport structures in two different rows on the same hemisphere are similar in shape, but their positions are different due to the meridional transport. We cross-correlate pairs of rows separated by heliographic latitude Δb in a sliding window with the size of 55 Carrington rotations. The edges of the correlation window are apodized by a smooth function to avoid the boxcar effects. The extremal position is calculated as a maximum of the parabolic fit of the set of correlation coefficients of correlated windows in five discrete displacements. If the distribution of the correlation coefficients does not have a maximum, or if the normalized quality of the fit is too low (under 0.8), the meridional velocity in this pixel is not evaluated. We have chosen $\Delta b = 5^\circ$ as the best tradeoff between the spatial resolution and precision.

To make the procedure more robust, we average the calculated meridional velocity for five consecutive rows separated by 0.5° and centered at Δb from the studied row. If any of the speeds in averaged five rows is far out of the expected range (-60 to $+60$ $\mathrm{m\,s^{-1}}$), then it is not used in the averaging. From the fit, the accuracy of the measured flow speed is evaluated and the maximum value of the set of five independent measurements at different rows is taken.

The same procedure is done with the processed map rotated by 180° to avoid any possible preferences in the direction determination, and both results are averaged. The measured errors were taken as the maximum value of both independent measurements.

For the ongoing analysis, only the speeds that were measured with the error lower than 3 $\mathrm{m\,s^{-1}}$ were taken into account. This criterion and some failures of the slope measurement introduce gaps in the data,

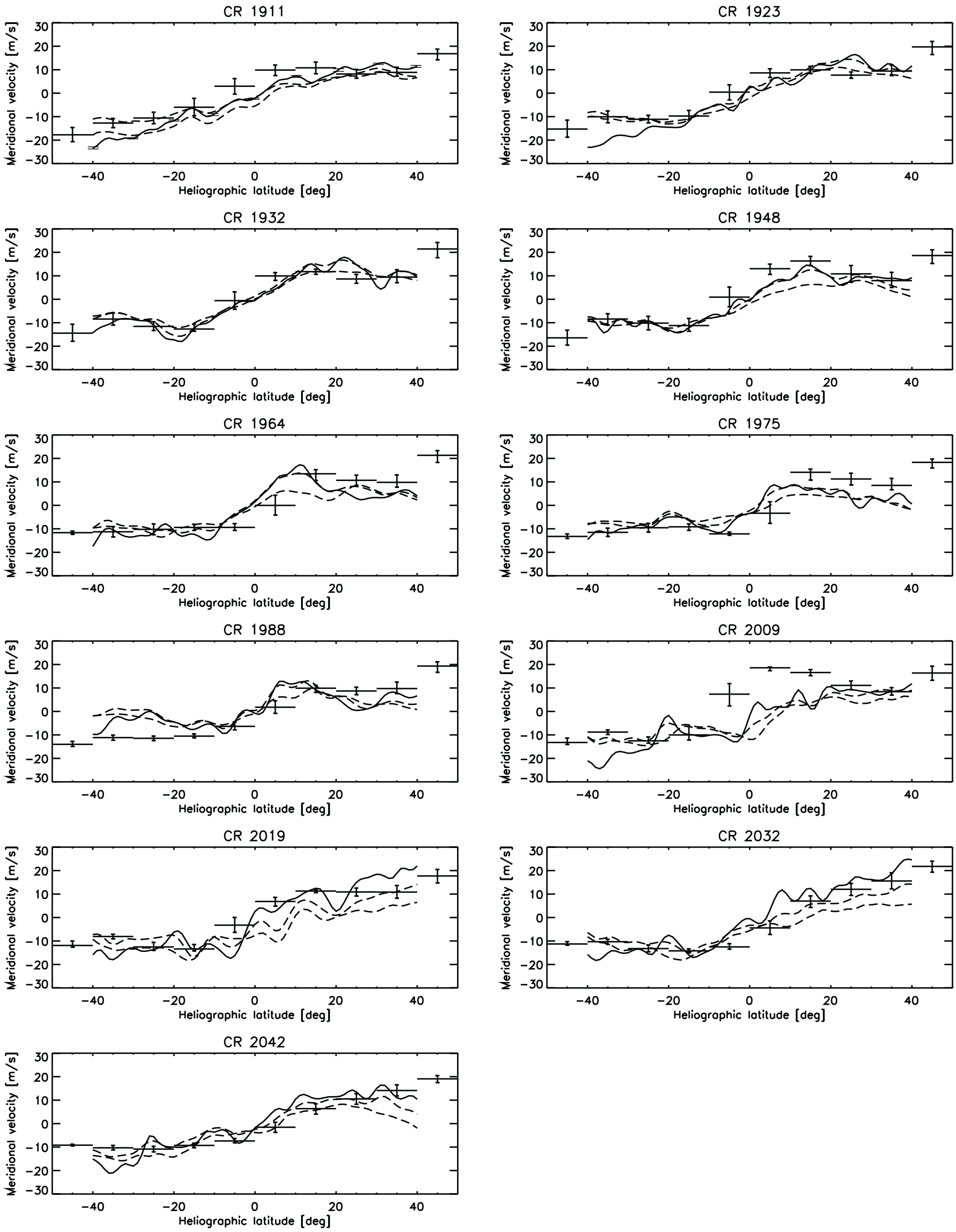

Figure 8: The longitudinally averaged meridional flow speed measured for a set of Carrington rotations by time-distance helioseismology. Solid line plots the time-distance mean meridional flow at 3–4.5 Mm depth, dotted at 6–9 Mm, and dashed at 9–12 Mm. The dots with error-bars represent the 10-degree-bin-averaged values of the flux transport speed derived from the magnetic butterfly diagram (Fig. 7*a*). Error bars of time-distance measurements are included for reference in CR 1911 (for details, see Zhao & Kosovichev, 2004).

which we need to fill. For this purpose we need to determine the best continuous differentiable field that approximates the data. The determination of such a field can be done in various ways, but we wish to avoid possible artifacts. For filling the gaps we used the MultiResolution Analysis. For details see Rieutord et al. (2007).

For the comparison between the meridional flow obtained from time-distance helioseismology (Zhao & Kosovichev, 2004) and the magnetic flux transport from our method, we have calculated the averaged values of both quantities in bins of 10 heliographic degrees. For the period of 1996–2006, only eleven

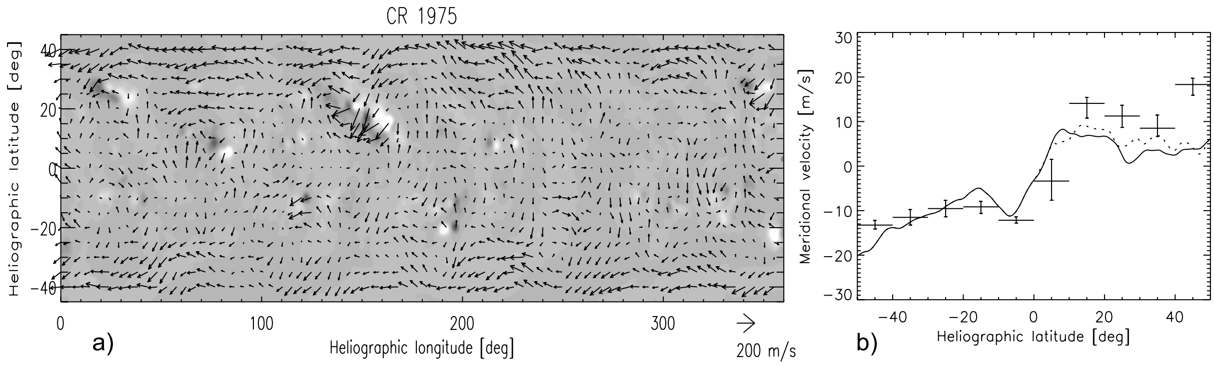

Figure 9: *a)* A large-scale flow map at depth 3–4.5 Mm for Carrington rotation No. 1975 (April 2001), the corresponding MDI magnetogram in the grey-scale background. Large-scale flows towards equator in the magnetic regions are visible around the large active region. *b)* The longitudinally averaged meridional circulation profile for the same Carrington rotation. The southern hemisphere depict almost no magnetic activity, so the meridional circulation profile obtained by averaging time-distance flow map (solid line) almost fits the magnetic flux transport profile (points with error-bars) there, while on the northern hemisphere they differ. After masking the magnetic regions on the northern hemisphere, the recalculated profile (dotted line) tend to fit to the butterfly tracking one also on the northern hemisphere.

Carrington rotations have been evaluated (one per year) by time-distance helioseismology using the full-disc *Dynamics data* from the MDI instrument on SoHO spacecraft. These data are available only for 60 days per year. We compared the measurements of the magnetic flux transport and the meridional flows in those particular non-consecutive Carrington rotations. The plots are displayed in Fig. 8.

The magnetic flux transport speed and the mean meridional flow speed obtained from helioseismology are very similar (correlation coefficients are in a range of 0.7–0.9). We have to keep in mind that while the time-distance meridional circulation profiles represents the behaviour of the plasma during particular Carrington rotations, the magnetic butterfly diagram tracking profiles represent the flux transport smoothed over 10 Carrington rotations, therefore the agreement cannot be perfect in principle. To make our results more accurate, the continuous helioseismic data are needed.

The speeds of the meridional flux transport in the near-equator region is less reliable, since the elongated structures in the magnetic butterfly diagram extend from the activity belts towards poles. In the equatorial region, significant part of the measurements were excluded from the analysis due to their large measured error. The gaps were filled using MultiResolution Analysis from well-measured points. Although the results seem reasonable here, we need to keep their lower reliability in mind. The original data are constructed from the images obtained with low resolution with the orthographical projection to disc. Therefore values above the latitude of $50\,^\circ$ are impacted by the projection effect, which reduces the spatial resolution and may cause an apparent increase of the measured meridional flux transport speed. This effect should be reduced if the higher resolution data would be used.

During the minimum of solar activity (such as CR 1911, 1923, or 2032), the profile of meridional flux transport speed is very consistent with mean longitudinally averaged profile of the meridional flow from helioseismology. The best agreement is found for depth of 9–12 Mm. This suggests that the flux transport may be influenced by flow in the deeper layers.

With increasing magnetic activity in the photosphere of the Sun, the gradient of the mean meridional circulation profile derived from time-distance helioseismology becomes steeper. This is consistent with the results obtained by numerical simulations by Brun (2004). The simulations show that with increasing magnetic activity, the Maxwell stresses oppose the Reynolds stresses, causing an acceleration of the meridional circulation and deceleration of the rotation in low latitudes. Our measurements show that the variations of the slope of the mean meridional flux transport speed in latitude with progression of the solar cycle are lower.

When the large-active regions emerge in the activity belt, the flow towards equator is formed on the equatorial side of the magnetic regions (see example of the subsurface flow map in Fig. 9*a*). This equatorward flow acts as a counter-cell of the meridional flow (present at the same longitudes as the corresponding magnetic region) and cause decrease of mean meridional flow amplitude in the activity belt. This behaviour is noticed in all studied cases recorded during eleven non-consecutive solar rotations, for which the Dynamics data useful for helioseismic inversion exist. Therefore the formation of the apparent counter-cell seems to be a common property of all large active regions in depths 3–12 Mm.

Flows in this counter-cell do not influence the magnetic flux transport, which can be demonstrated when the magnetic region is excluded in synoptic maps (Fig. 9*b*). The calculated meridional circulation profile is then closer to the profile of the meridional flux transport speed derived from the magnetic butterfly diagram.

7 Conclusions and perspectives

During my Ph. D. studies I have developed the method suitable for the measurements of horizontal velocity fields in the solar photosphere, which is based on the local correlation tracking (LCT) algorithm. The method consists of several separated steps covering the data processing procedure, including noise removal and coordinate transformations. The values of free parameters were adjusted using the synthetic data with known properties. They come from the SISOID numerical simulation, developed especially for this purpouse. From the comparison between the model velocity field and the calculated one the calibration curve was determined. At this point I have confirmed the fact that the LCT method underrepresents the magnitudes of the velocity field due to the spatial averaging during the calculation.

I have also compared the results of the proposed method with the results of time-distance local helioseismology, the method, which is considered the most powerfull in the topic of velocity fields measurements. It is shown that both methods reasonably match, which is encouraging for both methods.

The long-term behaviour of the surface flow field was studied. The generally accepted long-term properties were confirmed by the proposed method. The periodic analysis of the mean velocity components in the equatorial region did not show any conclusive results. We have detected few suspicious periods that might be related to the global Rossby waves pattern, but we cannot confirm this idea from the present material.

When a slightly modified version of the method was applied to the data describing the temporal evolution of solar photosphere under the filament in the time before and after its eruption, it was found that the topology of the surface flows have changed significantly. All the measured changes cause a stretch in the place, where the filament eruption started. The measurements support the theory of influence of the coronal magnetic field topology by the photospheric motions.

The study of the meridional flux transport measured from the magnetic butterfly diagram showed that the flux transport speed may significantly differ from the meridional speed of the plasma measured by the time-distance local helioseismology. The results suggest that in the dynamo models, the mean latitudinally averaged meridional flow speed coming from helioseismology cannot be used directly as the quantity describing the meridional flux transport. The longitudinal structure of the meridional flows seems to be very important.

7.1 Perspectives

The material obtained during the work related with this thesis provide a great perspective in the future investigations. In the future studies we would like to use it particularly for the investigation of the flows in active regions and of the coupling between the magnetic and velocity fields in magnetic areas. Especially, we will work on possible confirmation of the phenomenon of the dynamical disconnection of the sunspots from their magnetic roots, for which we believe that the current dataset is suitable.

By now, we have processed a three-day series of the great active region NOAA 9393, the largest active region of the current solar cycle, which are waiting for the detailed study, in which we would like to incorporate also the three-dimensional magnetic field reconstruction.

The filament eruption is a perfect material for the non-potential modelling of the coronal magnetic field and its evolution in time. We expect that it will provide a lot of information about the particular coupling of the magnetic field in corona and the horizontal photospheric large-scale flows.

The data coming from the magnetic butterfly diagram tracking analysis are suitable as an input for the flux transport dynamo models. We have started to cooperate with Dr. Mausumi Dikpati, an author of the well-behaving flux tranport dynamo model, which is able to reproduce the properties of last 12 solar cycles. We expect that the input of the real measured meridional flux tranport speed, which is essential, instead of that measured by local helioseimology will improve the results and the ability of the magnetic activity forecast. The longitudinal structure of the meridional flux transport speed and meridional flows need also a careful study.

Reference

Ambrož, P. 2001, Sol. Phys., 198, 253
Beck, J. G. 2000, Sol. Phys., 191, 47
Beck, J. G., & Schou, J. 2000, Sol. Phys., 193, 333
Brandenburg, A., & Subramanian, K. 2005, Phys. Rep., 417, 1
Brun, A. S. 2004, Sol. Phys., 220, 333
Carrington, R. C. 1859, MNRAS, 19, 81
Dikpati, M., de Toma, G., & Gilman, P. A. 2006, Geophys. Res. Lett., 33, 5102
Dikpati, M., & Gilman, P. A. 2006, ApJ, 649, 498
Georgobiani, D., Zhao, J., Kosovichev, A. G., Benson, D., Stein, R. F., & Nordlund, Å. 2007, ApJ, 657, 1157
Gizon, L., Duvall, T. L., & Schou, J. 2003, Nature, 421, 43
González Hernández, I., Komm, R., Hill, F., Howe, R., Corbard, T., & Haber, D. A. 2006, ApJ, 638, 576
Hart, A. B. 1956, MNRAS, 116, 38
Hathaway, D. H. 1988, Sol. Phys., 117, 1
Hathaway, D. H., Williams, P. E., & Cuntz, M. 2006, ApJ, 644, 598
Hindman, B. W., Gizon, L., Duvall, Jr., T. L., Haber, D. A., & Toomre, J. 2004, ApJ, 613, 1253
Howard, R., & Harvey, J. 1970, Sol. Phys., 12, 23
Hurlburt, N. E., Matthews, P. C., & Proctor, M. R. E. 1996, ApJ, 457, 933
Knaack, R., Stenflo, J. O., & Berdyugina, S. V. 2004, A&A, 418, L17
—. 2005, A&A, 438, 1067
Kosovichev, A. G. 1996, ApJ, 461, L55
Kuhn, J. R., Armstrong, J. D., Bush, R. I., & Scherrer, P. 2000, Nature, 405, 544
Leighton, R. B., Noyes, R. W., & Simon, G. W. 1962, ApJ, 135, 474
Mackay, D. H., & Gaizauskas, V. 2003, Sol. Phys., 216, 121
Mackay, D. H., & van Ballegooijen, A. A. 2006, ApJ, 642, 1193
November, L. J. 1986, Appl. Opt., 25, 392
November, L. J., & Simon, G. W. 1988, ApJ, 333, 427
Patsourakos, S., & Vial, J.-C. 2002, Sol. Phys., 208, 253
Rhodes, Jr., E. J., Korzennik, S. G., Hathaway, D. H., & Cacciani, A. 1991, in Bulletin of the American Astronomical Society, 1033
Rieutord, M., Roques, S., Roudier, T., & Ducottet, C. 2007, A&A, *in press*
Scherrer, P. H., Bogart, R. S., Bush, R. I., Hoeksema, J. T., Kosovichev, A. G., Schou, J., Rosenberg, W., Springer, L., Tarbell, T. D., Title, A., Wolfson, C. J., Zayer, I., & MDI Engineering Team. 1995, Sol. Phys., 162, 129
Schröter, E. H. 1985, Sol. Phys., 100, 141
Schüssler, M., & Rempel, M. 2005, A&A, 441, 337
Sobotka, M., Vázquez, M., Bonet, J. A., Hanslmeier, A., & Hirzberger, J. 1999, ApJ, 511, 436
Stellingwerf, R. F. 1978, ApJ, 224, 953
Title, A. M., Tarbell, T. D., Topka, K. P., Ferguson, S. H., Shine, R. A., & SOUP Team. 1989, ApJ, 336, 475
Toomre, J. 2002, Science, 296, 64
Švanda, M., Klvaňa, M., & Sobotka, M. 2005, Hvar Observatory Bulletin, 29, 39
Zhao, J., Georgobiani, D., Kosovichev, A. G., Benson, D., Stein, R. F., & Nordlund, Å. 2007, ApJ, 659, 848
Zhao, J., & Kosovichev, A. G. 2004, ApJ, 603, 776
Zhao, J., Kosovichev, A. G., & Duvall, Jr., T. L. 2001, ApJ, 557, 384

List of publications

Referee journals

1. **Švanda, M.**; Klvaňa, M.; Sobotka, M.: 2006, *Large-scale horizontal flows in the solar photosphere – I. Method and tests on synthetic data*, Astronomy & Astrophysics, **458**, p. 301–306
2. **Švanda, M.**; Zhao, J.; Kosovichev, A. G.: 2007, *Comparison of large-scale flows on the Sun measured by time-distance helioseismology and local correlation tracking*, Solar Physics, **241(1)**, p. 27–37
3. Kővári, Zs.; Bartus, J.; Strassmeier, K. G.; Vida, K.; **Švanda, M.**; Oláh, K.: accepted 21. 7. 2007, *Anti-solar differential rotation on the active K-giant σ Geminorum*, Astronomy & Astrophysics

Conference proceedings and contributions

1. **Švanda, M.**; Klvaňa, M.; Sobotka, M.; Bumba, V.: 2003, *Dynamics of motions in the quiet photosphere*, in Solar variability as an input to the Earth's environment. International Solar Cycle Studies (ISCS) Symposium (ESA SP-535), 23–28 June 2003, Tatranská Lomnica, Slovak Republic. Ed.: A. Wilson, p. 149–152
2. **Švanda, M.**; Klvaňa, M.; Sobotka, M.: 2005, *Motions of supergranular structures on the solar surface*, Hvar Obs. Bull., **29**, p. 39–48
3. Klvaňa, M.; **Švanda, M.**; Bumba, V.: 2005, *Temporal changes of the photospheric velocity field*, Hvar Obs. Bull., **29**, p. 89–98
4. **Švanda, M.**; Sobotka, M.; Klvaňa, M.: 2005, *Experiences with the use of the local correlation tracking method when studying large-scale velocity fields*, WDS'05 Proceedings of Contributed Papers: Part III – Physics (ed. J. Šafránková), Prague, Matfyzpress, p. 457–462
5. **Švanda, M.**; Klvaňa, M.; Sobotka, M.: 2005, *Mapping of large-scale photospheric velocity fields*, in Proceedings of the 11th European Solar Physics Meeting "The Dynamic Sun: Challenges for Theory and Observations" (ESA SP-600). 11–16 September 2005, Leuven, Belgium. Editors: D. Danesy, S. Poedts, A. De Groof and J. Andries. Published on CDROM, p. 71.1
6. Klvaňa, M.; Bumba, V.; **Švanda, M.**: 2006, *Doppler velocity fields in magnetic structures and their surroundings*, Cent. Eur. Astrophys. Bull., **30**, p. 21–30
7. Vida, K.; Kővári, Zs.; **Švanda, M.**; Oláh, K.; Bartus, J.; Strassmeier, K. G.: 2007, *Differential rotation and surface flow pattern on UZ Librae*, poster, 5th Potsdam Thinkshop – Meridional flow, differential rotation, solar and stellar activity
8. Kővári, Zs.; Bartus, J.; **Švanda, M.**; Vida, K; Strassmeier, K. G.; Oláh, K.; Forgács-Dajka, E.: 2007, *Surface velocity network with anti-solar differential rotation on the active K-giant σ Geminorum*, poster, 5th Potsdam Thinkshop – Meridional flow, differential rotation, solar and stellar activity
9. **Švanda, M.**; Kosovichev, A. G.; Zhao, J.: 2007, *Measurement of the meridional flux transport in the solar photosphere*, poster, 5th Potsdam Thinkshop – Meridional flow, differential rotation, solar and stellar activity

Submitted to referee journals

1. **Švanda, M.**; Klvaňa, M.; Sobotka, M.; Bumba, V.: submitted 25. 4. 2007, 2nd revision sent 28. 9. 2007, *Large-scale horizontal flows in the solar photosphere – II. Long-term behaviour and magnetic activity response*, Astronomy & Astrophysics
2. Roudier, Th.; **Švanda, M.**; Meunier, N.; Keil, S.; Rieutord, M.; Malherbe, J. M.;, Rondi, S.; Molodij, G.; Bommier, V.; Schmieder, B.: submitted 30. 5. 2007, 1st revision sent 14. 9. 2007, *Large-scale horizontal flows in the solar photosphere – III. Effects on filament destabilization*, Astronomy & Astrophysics
3. **Švanda, M.**; Kosovichev, A. G.; Zhao, J.: submitted 2. 9. 2007, 1st revision sent 28. 9. 2007, *Speed of meridional flows and magnetic flux transport on the Sun*, Astrophysical Journal Letters